AIAA JOURNAL
Vol. 46, No. 11, November 2008

Characterization and Aero-Optic Correction of a Forced Two-Dimensional Weakly Compressible Shear Layer

R. Mark Rennie,* Daniel A. Duffin,† and Eric J. Jumper‡
University of Notre Dame, Notre Dame, Indiana 46556

DOI: 10.2514/1.35290

Experimental data are presented consisting of fluid mechanic and optical measurements made in a forced two-dimensional weakly compressible subsonic shear layer. The measurements were made in the University of Notre Dame's compressible shear-layer facility that mixes high- and low-speed flows with speeds up to $M = 1.0$. The forcing was performed using voice-coil actuators mounted at the trailing edge of the splitter plate separating the high- and low-speed flows at the inlet to the mixing section. The experimental results are used to develop a simple yet effective feedforward adaptive-optic correction strategy for the optical aberrations imposed by the shear layer on a traversing laser beam.

Nomenclature

a	=	speed of sound
f	=	frequency
M	=	Mach number
M_{C2}	=	shear-layer convective Mach number
q	=	dynamic pressure
r	=	shear-layer velocity ratio, U_1/U_2
s	=	shear-layer density ratio, ρ_1/ρ_2
$\boldsymbol{S}$	=	strain-rate tensor
U_v	=	shear-layer convection velocity, $\sim 0.5(U_1 + U_2)$
u, U	=	streamwise root mean square, mean velocity component
x	=	streamwise distance from the splitter trailing edge
w, W	=	cross-stream root mean square, mean velocity component
y	=	spanwise location in the shear layer
z	=	cross-stream distance from the splitter trailing edge
z_B	=	z location at which $U = U_1 + B(U_2 - U_1)$
δ_ω	=	vorticity thickness, $(U_2 - U_1)/(\partial U/\partial z)_{\max}$
θ	=	momentum thickness
λ_2	=	lowest-valued eigenvalue of $\boldsymbol{S}^2 + \boldsymbol{\Omega}^2$
ρ	=	density
$\boldsymbol{\Omega}$	=	rotational tensor

Subscripts

f	=	forced
ff	=	far field
n	=	natural
rms	=	root mean square
1	=	low-speed flow
2	=	high-speed flow

Presented as Paper 4007 at the 38th AIAA Plasmadynamics and Lasers Conference, Miami, FL, 25–28 June 2007; received 24 October 2007; revision received 31 January 2008; accepted for publication 3 March 2008.

*Assistant Research Professor, Center for Flow Physics and Control, Department of Aerospace and Mechanical Engineering. Senior Member AIAA.

†Graduate Research Assistant, Center for Flow Physics and Control, Department of Aerospace and Mechanical Engineering. Member AIAA.

‡Professor, Center for Flow Physics and Control, Department of Aerospace and Mechanical Engineering. Fellow AIAA.

I. Introduction

TO MAXIMIZE the utility of aircraft-mounted laser systems, it is desirable that the system have as unrestricted a field of regard as possible. This objective is complicated by the fact that high-field-of-regard mounting arrangements typically generate a shear layer, associated with separated-flow regions, through which the beam must pass at high look-back angles. At subsonic and higher flight speeds, this shear layer becomes optically active, such that a laser beam passing through the shear layer will be distorted due to index-of-refraction variations within the flow. These index-of-refraction variations imprint a phase error, or aberration, onto the wave front of the laser beam, adversely affecting its far-field intensity pattern.

The phase characteristics of the initial light beam can be restored by placing the conjugate waveform of the aberration onto the optical wave front of the beam before its transmission through the aberrating flowfield. Systems that sense the aberration and construct and apply the proper conjugate waveform at regular time intervals are termed *adaptive-optic* (AO) systems [1]. For viewing through a high-subsonic-Mach-number shear layer, a successful adaptive-optic correction presents a serious problem because of the very high aberration frequencies involved. The effective bandwidth of contemporary closed-loop AO systems is generally less than 1 kHz [1,2], and this is not sufficient for the high-subsonic-Mach-number flows of interest.

One approach to the AO bandwidth problem is to increase the effective bandwidth of the AO system by regularizing the shear layer using controlled forcing inputs [3–7]. When forced, the turbulent energy of the shear layer goes preferentially into the formation of large-amplitude vortical structures, with passing frequency dictated by the forcing frequency, rather than into broadband turbulent fluctuations. Because these large-amplitude vortical structures are generated by the forcing input, the forcing signal can be used to determine the frequency and phase of the vortical structures, which now constitute the majority of the aberrating turbulent energy in the shear layer, over long distances within the shear layer. The forcing signal can thus be used to predetermine the shear-layer optical aberrations at any streamwise location and the AO deformable-mirror shapes required to correct them. In summary, although the turbulent frequency content of the shear layer is beyond the bandwidth of a *closed-loop* AO system, it is still well within the frequency capabilities of the deformable mirror alone; therefore, by forcing the shear layer, the shear-layer turbulence becomes more predictable, thus enabling AO control using a *feedforward* strategy.

The successful forcing of a two-dimensional weakly compressible subsonic shear layer was previously demonstrated in [5]. The shear layer was forced using voice-coil actuators that were mounted to the trailing edge of the splitter dividing the high- and low-speed flows and that vibrated in a direction normal to the flow direction. Optical

Malley-probe and wave-front data were presented that showed the regularized nature of the forced shear layer. In this paper, hot-wire data that are phase-locked to the forcing signal are presented that further characterize the nature of the forced shear layer. The shear-layer velocity data acquired from the hot-wire surveys are then used to interpret optical wave-front measurements made through the shear layer, leading to a novel and simple high-bandwidth AO correction of the regularized shear layer that implements the open-loop feedforward strategy described previously.

II. Approach

Experimental data were acquired in the University of Notre Dame's compressible shear-layer wind tunnel (CSLWT), which was constructed specifically to investigate the optical characteristics of high-subsonic compressible shear layers [5]. The CSLWT mixes codirectional high- and low-speed flows at high-subsonic flow speeds (M_2 up to Mach 1.0) to create a shear layer that is aero-optically active and representative of the kinds of aero-optic flows likely to be encountered on flight vehicles. The test section of the CSLWT is 900 mm in length, and the low-speed side of the test section contracts at an angle of 6.3 deg in the flow direction to reproduce the streamwise pressure and mass-flow distribution of a free shear layer in unconstrained flow [3,8]. Wall effects cannot be completely compensated in the facility design, however, because the wall on the high-speed side of the jet acts like a reflection plane, such that the shear layer within the test section effectively behaves like one side of a planar jet. These wall effects become more important as the shear layer grows in the streamwise direction, such that it was judged that the preferred region for testing was $x \lesssim 550$ mm. Despite this limitation, the measured static pressure within the CSLWT test section is constant in the streamwise direction to within $\pm 0.003q$, and the success of the CSLWT in creating a physically realistic shear-layer flow was confirmed by fluid mechanic and optical measurements. Details of the unforced-shear-layer flow in the CSLWT can be found in Appendix A.

Measurements for this investigation included hot-wire surveys of the CSLWT velocity field and optical measurements of the aberrations caused by density variations within the shear-layer flow. The hot-wire measurements were made using a constant-temperature cross-wire probe with 5-μm-diam tungsten wires that were welded to the probe supports. This probe was prone to breakage within the shear layer, probably due to the thermal wake of the probe passing over the wire weld points when the probe was in regions of high flow angles, and more robust wires/films or attachment strategies were not investigated. To reduce the number of hot-wire breakages to acceptable levels, the hot-wire measurements were made at a high-speed-flow Mach number of $M_2 = 0.35$. To increase compressibility effects and thus density variations and optical signal-to-noise ratio, the optical measurements were made at a high-subsonic wind speed of $M_2 = 0.78$. The shear-layer velocity ratio was $r \approx 0.15$, which is representative of shear layers associated with separated-flow regions, and is similar to r values used in other investigations [9]. Based on the results of the hot-wire surveys, the shear layer was estimated to be turbulent for all test cases. A schematic of the CSLWT test section including hot-wire and optical measurement locations is shown in Fig. 1.

The importance of compressibility effects on the development of the shear layer in the CSLWT was evaluated by computing the convective Mach number M_{C2} [10] for each test condition:

$$M_{C2} = (U_2 - U_C)/a_2 \tag{1}$$

where

$$U_C = \frac{a_2 U_1 + a_1 U_2}{a_1 + a_2} \tag{2}$$

The maximum value of the convective Mach number occurred for optical measurements that were made at $M_2 = 0.78$. The convective Mach number for this test condition was $M_{C2} = 0.32$, which is still sufficiently low that flow compressibility can be assumed to have had no effect on the shear layer spreading [10]. As shown in [11], the flow in the CSLWT can therefore be considered to have been weakly compressible in the sense that, although density variations exist at higher values of M_2, compressibility effects are essentially decoupled from the kinematic properties of the underlying shear flow. This decoupling of compressibility effects from the flow kinematics means that the hot-wire measurements made at $M_2 = 0.35$ can still be used to infer the velocity field that existed in the higher-speed $M_2 = 0.78$ flow used for the optical measurements.

The approach used to force the CSLWT shear layer was based on published data [3,6,12] showing that a shear layer is most susceptible to forcing at the trailing edge of the splitter between the high- and low-speed flows and in a direction perpendicular to the flow direction. Following this approach, two different splitter-plate inserts were constructed: one using voice-coil actuators and a second using piezoelectric strip actuators mounted at the splitter trailing edge. These types of actuators were chosen because of their ability to generate useful forcing displacements at the high frequencies necessary to force the high-speed flows of interest. Both of these inserts were successfully used to force the shear layer; however, the voice-coil splitter was used for most of the testing because of its ease of use, larger frequency bandwidth, and higher maximum useful forcing frequency. As shown in Fig. 2, the voice-coil actuator splitter consisted of clipped miniature speakers mounted so that the exposed diaphragms applied a perturbation perpendicular to the flow direction on the high-speed side of the splitter trailing edge. The amplitude of the vertical motion of the voice-coil diaphragms, measured without flow using an optical technique, was approximately 0.7 mm at 350 Hz, decreasing to 0.2 mm at 750 Hz. The maximum frequency at which robust forcing of the $M_2 = 0.78$ flow could still be achieved was approximately 800 Hz. Additional details on development of the forcing actuator are presented in [5].

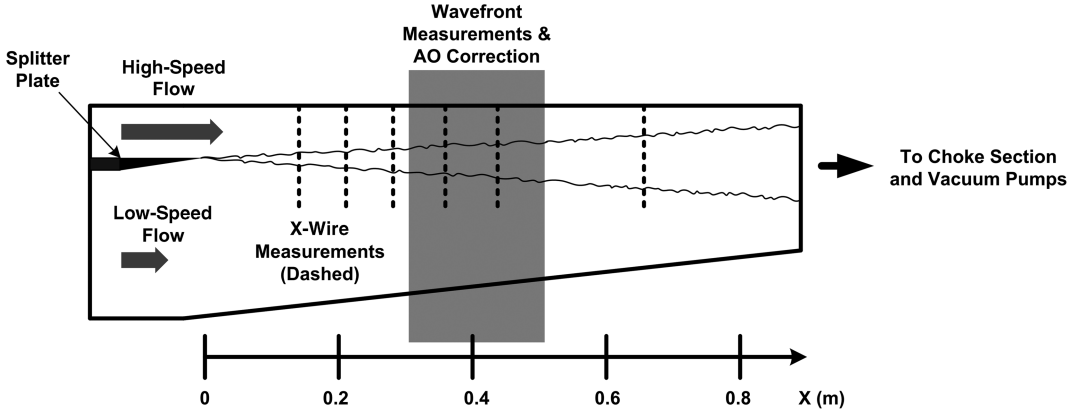

Fig. 1 Schematic of the CSLWT test section showing measurement locations.

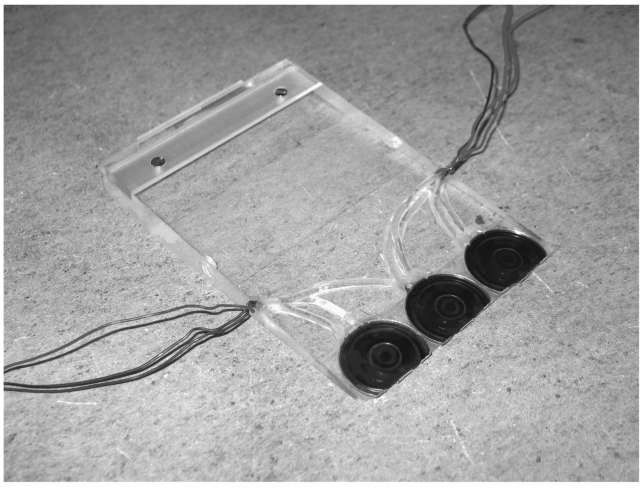

Fig. 2 Photograph of forcing actuator, consisting of clipped, 36-mm-diam speakers mounted to trailing edge of shear-layer splitter plate.

III. Results

A. Forced Shear Layer

The approach used to force the shear layer was based on the significant body of literature that indicates that far-downstream regularization of a shear layer can be achieved by forcing at a single frequency only [3–7]. According to [3], when forced at a single frequency, the shear layer achieves a structure size and passing frequency that is dictated by the forcing frequency at a location that is upstream of where it would occur in the unforced shear layer. This enhanced growth region is followed by a regularized region in which vortex pairing is suppressed and the shear layer is characterized by a coherent train of vortex structures. More important, in the regularized region of the shear-layer, broadband turbulent fluctuations are suppressed below levels existent in the unforced shear layer, because turbulent energy is drawn preferentially into the formation of the large vortical structures. The regularized region is maintained until the location at which $f_f = f_n$, at which point the shear layer resumes its normal growth.

The key to any single-frequency forcing strategy is therefore that the forcing frequency should be selected to correspond to the natural frequency of the shear layer at the *farthest downstream* location at which regularization of the shear layer is required. The shear-layer natural frequency as a function of streamwise location was measured using a Malley probe, which is a nonintrusive instrument that senses the deflection caused by the shear layer on a small-aperture beam of light that traverses the flow [13]. The Malley-probe jitter signal is directly related to the turbulent content of the flow by well-established fluid mechanic linking equations [14]. In Fig. 3, the shear-layer natural frequency, taken as the peak spectral frequency of the Malley-probe jitter data, is plotted as a function of streamwise location x. Figure 3 shows that the natural frequency of the shear layer ranges from several hundred hertz to a few kilohertz over the extent of the CSLWT test section.

Using the shear-layer natural-frequency data shown in the Fig. 3, the target location for shear-layer regularization was chosen to optimize the experimental conditions: in particular, the limit on forcing frequency in the $M_2 = 0.78$ flow to less than approximately 800 Hz and the preference for testing in the region $x \lesssim 550$ mm to avoid excessive wind-tunnel-wall effects. Figure 3 shows that the shear-layer location that meets these two restrictions occurs in the region $x \approx 500$ mm, where the shear-layer natural frequency is approximately 750 Hz. Using $x = 500$ mm as an optimum test location is also justified from an aero-optic standpoint, because it lies some distance downstream of the splitter trailing edge, where shear-layer structures have grown to a size at which they produce significant optical aberrations. As such, aero-optic testing in the region $x \approx 500$ mm simulates a fairly moderate look-back angle at which the aero-optic problem would become an important parameter for airborne laser systems.

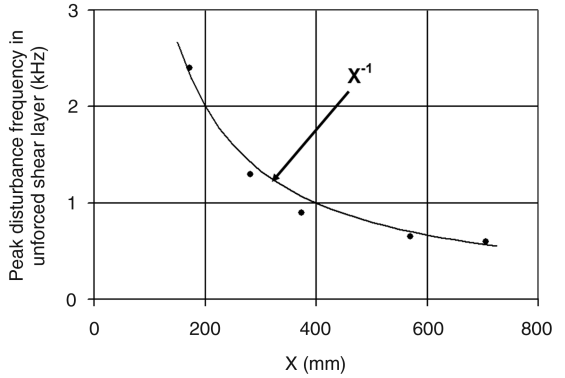

Fig. 3 Streamwise dependence of the peak spectral frequency in the unforced shear layer [5]; $M_2 = 0.78$.

Momentum-thickness growth for single-frequency forcing at 750 Hz are shown in Fig. 4. Because the cross-wire data were acquired at a lower speed than used for the optical measurements shown in Fig. 3 (i.e., $M_2 = 0.35$ rather than $M_2 = 0.78$), the 750 Hz natural frequency from Fig. 3 was scaled by the wind speed to obtain a forcing frequency of $f_f = 340$ Hz. Figure 4 shows that the single-frequency forcing resulted in enhanced shear-layer growth, indicating shear-layer regularization, and that the region of enlarged θ was maintained up to the target location of $x \approx 500$ mm, the point at which f_f was selected to match f_n.

Power spectra of velocity fluctuations measured in the unforced and forced shear layers are compared in Fig. 5 for different streamwise locations x. The spectra were taken inside the turbulent region of the mixing layer at a z location aligned with the level of the splitter. As expected, the frequency content of the unforced shear

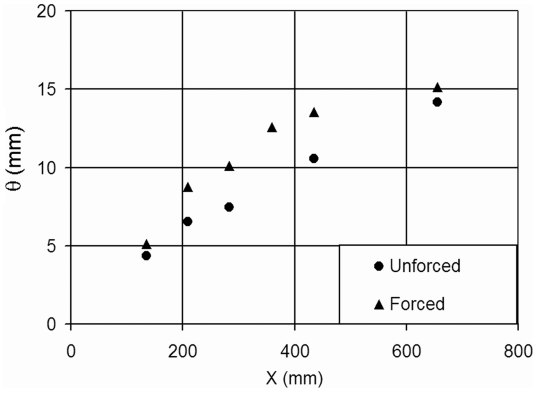

Fig. 4 Shear-layer momentum thickness spreading in CSLWT; $M_2 = 0.35, f_f = 340$ Hz.

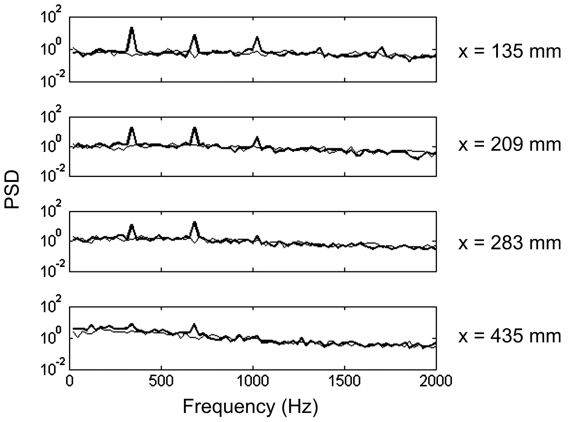

Fig. 5 Velocity spectra for unforced (solid) and forced (bold) shear layers; $M_2 = 0.35$.

layer shifts to lower frequencies with increasing streamwise distance x. In all cases, the forced-shear-layer spectra show strong peaks at the 340 Hz forcing frequency, and Fig. 5 shows that the goal of matching the forcing frequency to the shear-layer dominant frequency at $x \approx 500$ mm was achieved. Several harmonics of the forcing frequency are also visible in the forced spectra. Measurements made without flow showed that the voice-coil actuator motion was almost a pure sine wave; however, it is possible that the actuator motion could have been altered in the high-speed flow of the wind tunnel. As such, it cannot be clearly determined whether the harmonics that appear in Fig. 5 were introduced by the actuator or were generated by the shear layer itself as the residual signal of upstream vortex-pairing events. Also visible in Fig. 5 is an indication of a 170 Hz subharmonic to the 340 Hz forcing signal in the spectrum at $x = 435$ mm. The presence of the forcing subharmonic at this location concurs with the results of vortex mapping and optical measurements shown later.

As a final check of the effectiveness of the shear-layer forcing, nondimensional Reynolds-stress profiles were computed from the forced and unforced hot-wire data and are shown in Fig. 6. The figure shows a monotonic increase in the Reynolds stress of the unforced shear layer between successive downstream measurement locations, but a marked reduction in Reynolds stress in the forced shear layer from $x = 135$ to 283 mm. In [15] it is shown that a reduction in Reynolds stress occurs at the completion of a vortex-pairing process. As such, Fig. 6 indicates that coherent vortex pairing in the forced shear layer must have occurred in the region $x = 135$ to 283 mm, which is consistent with the start of the regularized region shown by the momentum-thickness measurements (Fig. 4). Furthermore, at the farthest downstream location, the Reynolds stresses in the forced shear layer are lower than in the unforced case. In [16] it is shown that the Reynolds stress is physically linked to the shear-layer momentum-thickness growth rate and indicates the direction of energy exchange between the shear layer and the mean flow. In extreme cases of large-amplitude forcing [3,6], the shear layer actually contracts in the regularized region and the Reynolds stress reverses sign, indicating transfer of energy from the shear layer back to the mean flow. As such, the results of this section confirm that the forced shear layer in the CSLWT was regularized, but that the level of forcing provided by the actuator might be considered moderate in the sense that the shear-layer forcing achieved a reduction, but not a reversal, of the Reynolds stresses.

B. Vortex Topology

Further insight into the physical processes occurring in the forced and unforced shear layers was obtained by computing vortex distributions from the measured velocity data. The method used to identify vortex location was the lambda-2 method [17]. This method is derived from the vorticity transport equation, which is used to determine a condition for the existence of local pressure minima due to vortical motions only. In two-dimensional flow, this condition is satisfied when the lowest-valued eigenvalue (i.e., λ_2) of the tensor $\boldsymbol{S}^2 + \boldsymbol{\Omega}^2$ is negative.

Lambda-2 distributions of the forced and unforced shear layers are shown in Fig. 7. The distributions were computed from velocity data measured using a single cross-wire probe that was vertically traversed through the flow at the locations $x = 135$, 209, 283, 359 (forced-case only), 435, and 655 mm. For the forced shear layer, the forcing signal was recorded (shown at the bottom of the figure) and phase-lock-averaged velocity profiles were determined for several phases of forcing at each measurement station. The space between the measurement stations was interpolated by making a quasi-frozen-flow assumption, whereby phase-locked velocity profiles were propagated upstream and downstream from each measurement station at the mean vortex convection speed U_v until they merged with the data from neighboring measurement stations. The λ_2 distribution for the forced shear layer clearly shows large contiguous regions over which λ_2 is negative (dark regions in Fig. 7b) and which can be identified as vortices. The presence of these clearly discernible vortices in the phase-locked data provides convincing evidence that the forced shear layer is characterized by long-term coherent vortex formation locked to the forcing signal.

For the unforced shear layer, a 340 Hz signal was also recorded for reference (although the forcing actuators were not energized). This signal was also used to phase-lock and interpolate the unforced data in the same way as the forced data. Although the λ_2 distribution for the unforced case shows some interesting cross-stream variation, there are no clear concentrations in the streamwise direction to indicate any vortex passing that is phase-locked to the 340 Hz reference signal. Because the shear layer was not actually forced, there is no reason to expect that vortex shedding would be phase-locked to 340 Hz or any other frequency; however, Fig. 7a provides an illustration of the kind of λ_2 distribution that results for incoherent vortex shedding in the unforced shear layer, in contrast to Fig. 7b.

The forced λ_2 distribution in Fig. 7b shows three vortices at $x \approx 175$, 250, and 450 mm. The vortices are separated by braids, shown in light, at $x \approx 200$, 325, and 550 mm. With reference to the forcing signal plotted on the bottom of the plot, the first two vortices are separated by a distance roughly equal to half the forcing wavelength, and the second two vortices are separated by the forcing wavelength. Based on this change in phase-locked vortex spacing, consistent vortex pairing can be inferred to occur roughly in the vicinity of the second vortex at $x \approx 250$ mm. Vortex pairing in this region agrees with the results of the momentum-thickness and Reynolds-stress measurements shown in Figs. 4 and 6.

Two additional observations can be made regarding the forced λ_2 distribution in Fig. 7b. First, the third vortex at $x \approx 450$ mm appears significantly weaker than the first two, and second, the third vortex also appears to consist of at least two smaller vortices. The smaller vortices at the third location suggest that a vortex-pairing event is occurring here; however, it must be remembered that Fig. 7b was computed from phase-lock-averaged data and that the appearance of multiple vortices can also be produced by a single vortex shifting to different positions at different cycles of the forcing. Shifting of the vortex location from cycle to cycle would result if the shear-layer

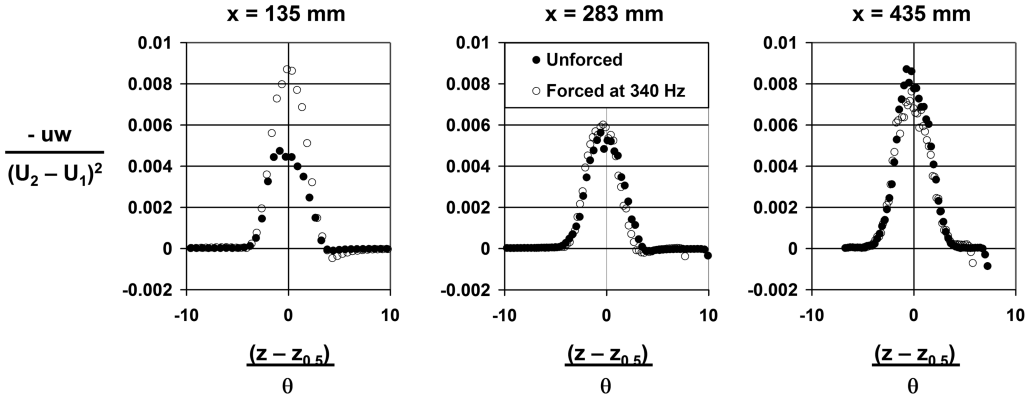

Fig. 6 Reynolds-stress profiles measured in the CSLWT; $M_2 = 0.35$.

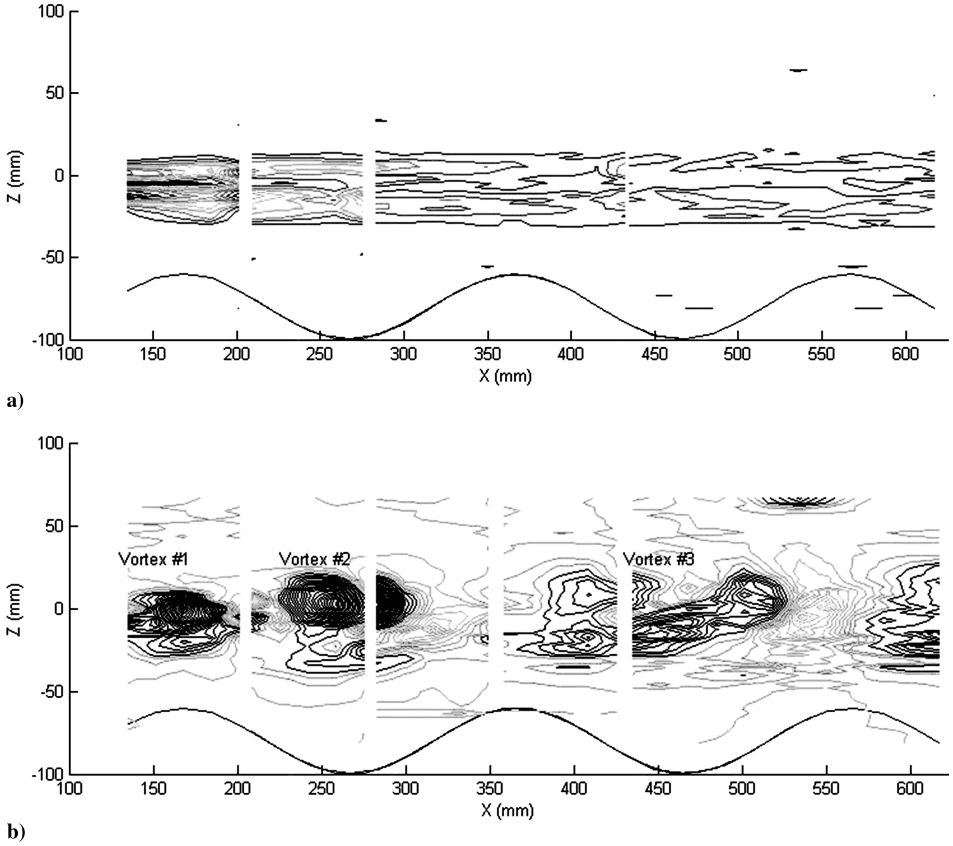

Fig. 7 λ_2 distributions in the a) unforced and b) forced shear layers; $M_2 = 0.35$.

response contained a significant frequency component at the forcing subharmonic, which would also produce the appearance of weaker vortex strength when many cycles are averaged, as in Fig. 7.

This kind of multicycle periodicity in the vortex topology has been reported in our previous computational studies using a discrete-vortex method (DVM), which has been used to successfully model the features of incompressible and weakly compressible experimental shear flows [13,18–20]. The DVM computes the shear-layer velocity field using two-dimensional discrete vortices that are allowed to freely convect under the net induced velocity imposed by all other vortices residing in the computational domain added to the overall mean flow speed. This kind of computation of the shear-layer velocity field in the absence of compressibility effects is warranted because of the low convective Mach number of the experimental flow being modeled. Figure 8 shows successive realizations of the discrete-vortex loci at the same forcing phase angle, computed using the DVM for conditions approximating the experimental forced shear layer shown in Fig. 7b. The figure clearly shows that the discrete-vortex distribution resembles itself at every other cycle of the forcing, rather than at every cycle. In Fig. 8, an arbitrarily large computational forcing amplitude was used to make the discrete-vortex patterns more apparent; however, the subharmonic dependence of the vortex distribution can be discerned at all levels of forcing. It is obvious that phase-lock averaging of the data shown in Fig. 8, without accounting for the 2-cycle subharmonic periodicity of the flow, would give a false impression of the strength and location of the vortices in the flow.

In summary, the presence of coherent vortices in the experimental vortex distribution, phase-locked to the forcing signal, further demonstrates the regularized nature of the experimental forced shear layer. Of equal significance, the experimentally measured vortex distribution and computed DVM results for the forced shear layer both suggest that the aero-optic region of interest from $x \approx 200$ to 500 mm is dominated by structure passing at the fundamental and subharmonic of the forcing frequency. Higher-order harmonics of the forcing do not appear to play a significant part in the vortex

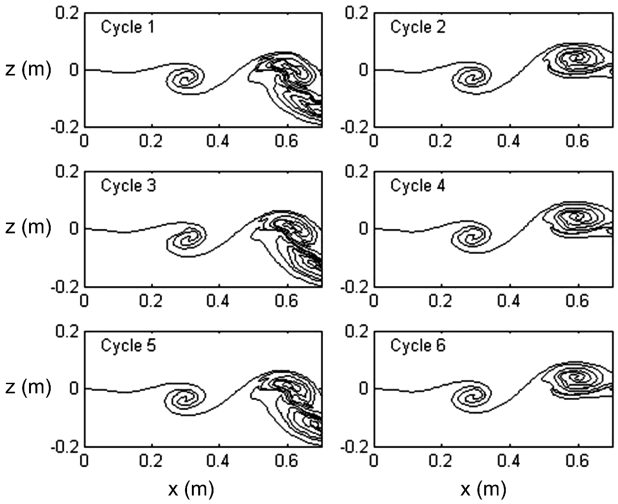

Fig. 8 Six successive realizations of the discrete-vortex loci computed using discrete-vortex method for the forced shear layer; $M_2 = 0.35$.

topology of this region, despite the presence of noticeable harmonic content in the hot-wire velocity spectra shown in Fig. 5. As will be shown next, this predominant fundamental-subharmonic frequency content of the forced shear layer is confirmed by aero-optic measurements.

C. Adaptive-Optic Correction

Our investigations into the forcing of high-subsonic compressible shear layers were motivated by the goal of increasing the bandwidth of adaptive-optic correction systems. In this regard, the best evaluation of the level of success in regularizing the forced shear layer ultimately comes from optical measurements, because fluid

mechanic measurements may not give an accurate representation of optical aberrations caused by the shear layer. In particular, small structures that produce strong high-frequency turbulence may not produce significant optical aberrations when their aberrating effects are integrated to determine optical path length. As such, the turbulence spectra in Fig. 5 may not accurately represent the important frequency content or phase relationship of the associated optical aberrations.

Optical wave fronts were measured using a Shack–Hartmann-type wave-front sensor manufactured by Wavefront Sciences. The flow was interrogated using a 532 nm wavelength frequency-doubled Nd: YAG laser beam that was apertured to a 200 mm diameter before passing through the shear-layer flow between the stations $x = 300$ to 500 mm. Referring to Fig. 7, this aperture size coincidentally matched the structure wavelength in the regularized shear layer. The wave-front sensor was a charge-coupled device (CCD) camera with a 33×44 lenslet array, and although the frame rate of the CCD camera was only 30 Hz, the $M_2 = 0.78$ flow was effectively frozen by the 8 ns laser pulses.

Phase-lock-averaged wave fronts acquired for 90 deg viewing through the forced shear layer are shown in Fig. 9 [21]. The wave fronts show the optical path difference (OPD) at each location of the laser beam after passing through the flow, plotted over the 200-mm-diam aperture of the laser beam. Wave fronts are shown for 60 deg separations in the phase of the forcing cycle and clearly show a sinusoidal variation of the optical wave front over the viewing aperture, in phase with the forcing. To capture any subharmonic dependence of the shear-layer aberrations, Fig. 9 also shows wave

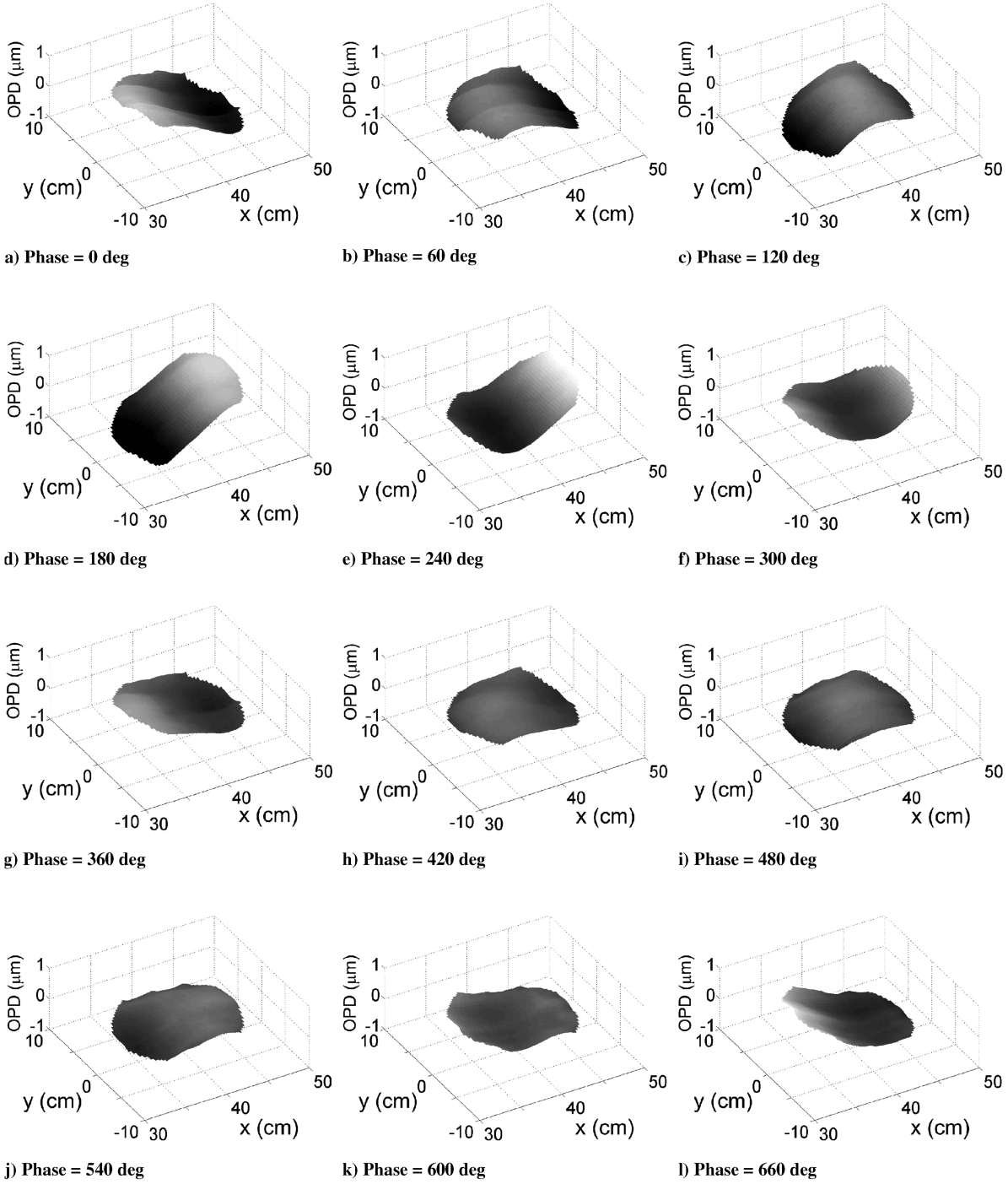

Fig. 9 Two-cycle, phase-lock-averaged wave fronts measured for normal-incidence viewing through the shear layer forced at a single frequency; $M_2 = 0.78$ and $f_f = 750$ Hz.

fronts for two cycles of the forcing signal, phase-locked to the forcing subharmonic. Comparison of the wave fronts between the first and second forcing cycles in Fig. 9 shows that although they retain the same overall sinusoidal variation in each cycle, the wave fronts display noticeable differences between the first and second phase-locked cycles, suggesting a two-cycle subharmonic periodicity to the optical aberrations produced by the shear layer.

To gain further insight into the composition of the forced-shear-layer aberrations, a proper orthogonal decomposition (POD) [22] of the measured wave fronts was undertaken. The first 8 modes of the POD are plotted in Fig. 10, and the cumulative energy in the POD modes is shown in Fig. 11. The figures show that the first two modes, which account for almost 90% of the optical aberration, are almost completely two-dimensional, with only small variations in the cross-stream direction and, furthermore, that the first two modes can be closely approximated by sine waves with wavelengths of twice the aperture size (mode 1) and equal to the aperture size (mode 2). Because, as mentioned previously, the interrogating-aperture diameter matched the forcing wavelength, the POD results show that the majority of the optical aberration is contained in two-dimensional sinusoidal variations at the subharmonic (mode 1) and fundamental (mode 2) of the forcing frequency. This two-cycle periodicity in the shear-layer optical aberration is consistent with the subharmonic interpretation of the measured vortex topology shown in Fig. 7 and the predictions of the DVM shown in Fig. 8.

The relative simplicity of the mode structure of the optical aberrations suggested that a very simple yet effective AO correction of the forced-shear-layer aberrations could be achieved by compensating the first two POD modes of the forced aberration only. A schematic showing the approach for this kind of feedforward AO correction is shown in Fig. 12. The correction proceeds by first preprogramming the AO deformable mirror to apply the conjugate of the first two POD modes of the forced-shear-layer aberration (Fig. 10). Because these modes are well approximated by two-dimensional sinusoids at the subharmonic and fundamental components of the forcing frequency, they are easy to preprogram into the AO deformable-mirror (DM) control hardware and can be reproduced with little stress to the DM reflective membrane. The preprogrammed DM deflections are then phase-locked to the shear-layer aberrations using a synchronizing signal from the shear-layer

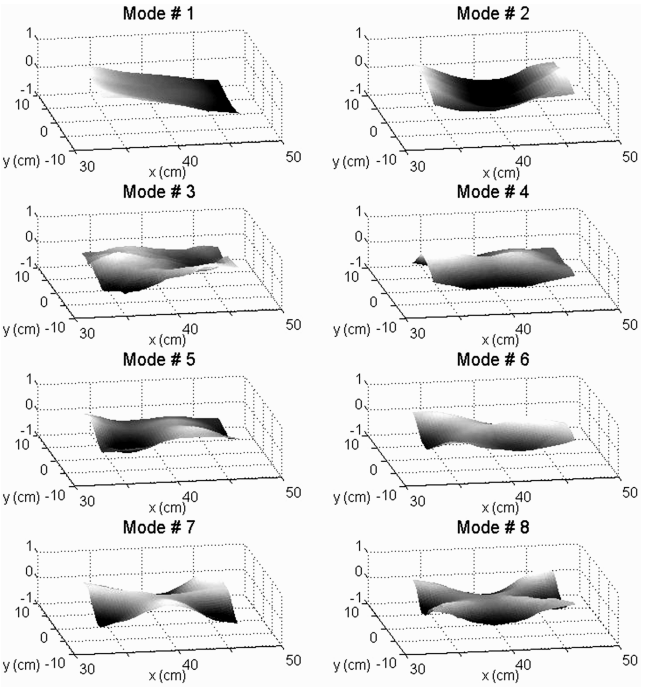

Fig. 10 Isometric view of the first eight normalized POD modes of the optical aberration for 90 deg viewing through the forced shear layer.

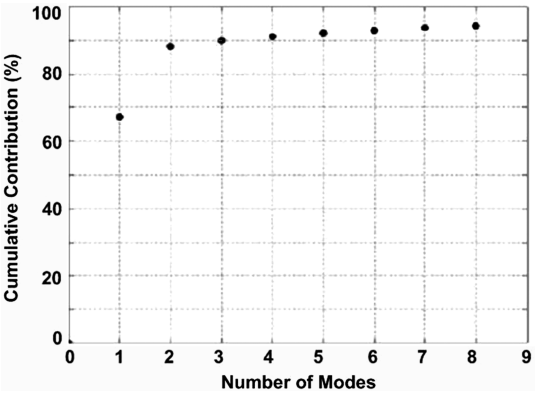

Fig. 11 Cumulative contribution of the first eight POD modes to the overall measured optical aberration for 90 deg viewing through the forced shear layer.

forcing actuator. The incoming laser beam is then reflected from the DM before passing through the regularized shear layer, in effect, preconditioning the beam with the conjugate to the aberrating effect of the forced shear layer. As such, when the preconditioned laser beam passes through the shear layer, the shear-layer aberrations restore the wave fronts of the laser beam to nearly their initial planar character.

This type of feedforward AO correction, shown in Fig. 12, was recently conducted at the University of Notre Dame [21]. The correction used Notre Dame's adaptive-optic correction system, which was manufactured by Xinetics Corporation. The system is built around a 50-mm-diam deformable mirror that is controlled using 37 piezoelectric actuators; this DM is capable of accurately reproducing waveforms with frequencies up to approximately 1 kHz. When operated in its normal feedback-control setup, the Xinetics system includes a separate wave-front sensor that measures the optical aberrations, computes a correction, and feeds back control signals to the DM. However, due to latencies associated with the control hardware and amplifiers, the AO system as a whole is capable of closed-loop corrections of optical aberrations with frequency content up to only around 50 Hz. This correction frequency is far too low to compensate the aberrations in a transonic aero-optic flow such as the CSLWT shear layer and emphasizes the advantage of the feedforward approach shown in Fig. 12.

The Xinetics system was converted for feedforward control by disconnecting the normal feedback loop, preprogramming the DM control hardware to reproduce the first two forced-shear-layer mode shapes shown in Fig. 10, and connecting a synchronizing signal to the forcing actuator. Because the required DM shapes were only two-dimensional (that is, modes 1 and 2 of Fig. 10), the DM actuators

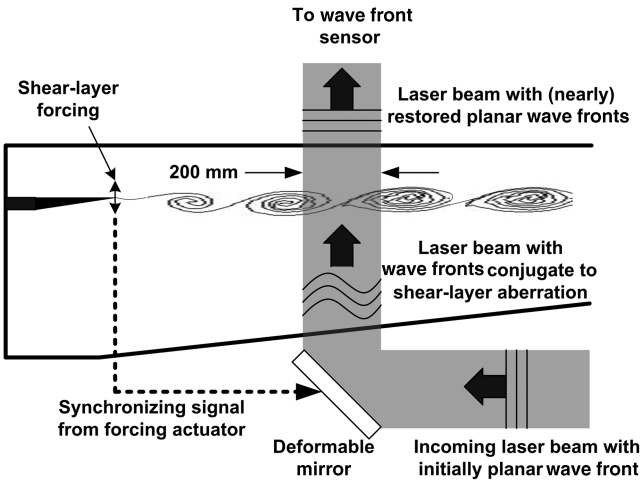

Fig. 12 Schematic of feedforward adaptive-optic correction.

Table 1 Figures of merit for experimental feedforward AO correction [21]

	Unforced shear layer	Forced shear layer	AO-corrected
OPD_{rms}	0.263	0.385	0.102
Strehl ratio[a]	0.137	0.076	0.660

[a]Strehl ratios are shown for standard 1.0 μm wavelength radiation.

aligned perpendicularly to the flow direction were linked together so that, in practice, the DM was reduced to just 7 active strips. Test beams reflected from the DM showed that the DM could reproduce the wave fronts required to correct the forced-shear-layer aberrations to within an average spatial OPD_{rms} error of 0.038 μm. The AO corrections were made using a 532 nm wavelength Nd:YAG laser beam; after reflecting from the DM, the laser beam was expanded to a 200 mm diameter and passed through the shear layer between the locations $x = 300$ to 500 mm.

One of the greatest difficulties of the correction strategy was fine-tuning the synchronization of the preprogrammed fundamental/subharmonic DM motion with the shear-layer aberration. Strategies are currently under development to achieve phase-locking and even amplitude adjustment between the DM and the forced aberrations using a simple high-bandwidth optical instrument such as a Malley probe; however, for this experiment, open-loop feedforward control was used in the sense that only the forcing signal was used to synchronize the DM. As such, to ensure that the preprogrammed DM motions would be phase-locked to the subharmonic of the aberrations, a small-amplitude subharmonic component, with an amplitude of only 10% of the amplitude of the fundamental component, was added to the forcing signal. This subharmonic component facilitated phase-locking of the DM with the aberrations by stabilizing the two-cycle repetition of the aberrations.

Figures of merit for the experimental feedforward AO correction are presented in Table 1. The table shows values for the spatial OPD_{rms} over the aperture of the laser beam for viewing through the unforced and forced shear layers, as well as for viewing through the forced shear layer using the feedforward AO correction. The OPD_{rms} values shown in Table 1 have been adjusted to remove the aberrating effect of the high-speed compressible boundary layer on the roof of the CSLWT test section. Large OPD_{rms} values negatively impact the ability to focus the laser beam in the far field, and a more informative measure of the effectiveness of the AO correction is the Strehl ratio, which gives the ratio of the peak on-axis intensity of the focused beam to the optimum diffraction-limited intensity. As shown in the table, the correction reduced the OPD_{rms} of the aberration to less than 50% of that measured in the original unforced shear layer, whereas the Strehl ratio was improved by almost 5 times to 0.66. Time-averaged far-field irradiance patterns for the feedforward AO-corrected and unforced shear layers are shown in Fig. 13, which includes rings showing the extent of the Airy disk, with radius r_A, for the unaberrated beam. Figure 13 clearly shows the improvement realized by this simple AO correction strategy.

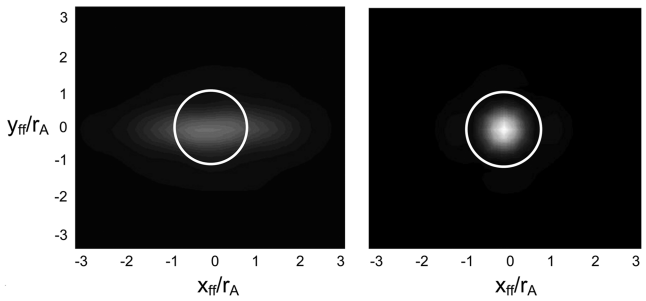

Fig. 13 Time-averaged far-field irradiance patterns for a laser beam transiting the unforced shear layer (left) and the forced shear layer with feedforward AO correction (right).

IV. Conclusions

Regularization of a weakly compressible $M_2 = 0.78$ shear layer by forcing applied at the splitter trailing edge was confirmed by hot-wire and optical measurements. The behavior of the forced shear layer conforms to trends already reported in the literature; however, it is noteworthy that previous studies have generally been confined to much-lower-speed incompressible flows. As such, the results reported here make a valuable addition to the forced-shear-layer literature.

An important outcome of the investigation is that the downstream region of the forced shear layer, which is of particular interest for aero-optic applications, is governed predominantly by fluctuations at the fundamental and subharmonic of the forcing frequency. This outcome is confirmed by the measured and numerically computed vortex topology as well as by wave-front measurements on a beam of light that traversed the flow.

The simplicity in the frequency content of the optical aberrations of the forced shear layer enabled a simple feedforward AO correction strategy that was successfully used to realize a fivefold improvement in the Strehl ratio of a laser beam transiting a $M_2 = 0.78$ and $M_1 = 0.12$ shear layer with optical aberration frequencies from at least several hundred hertz to a few kilohertz. To our knowledge, this is the first adaptive-optic correction demonstrated for an aberrating flow with such large amplitude and, more important, such high-frequency content of optical aberrations.

Appendix A: Characterization of the Unforced Shear Layer

Velocity profiles measured within the unforced CSLWT shear layer at several streamwise locations are plotted in Fig. A1. The profiles, plotted using nondimensional similarity parameters, show that the unforced shear layer exhibits a self-preserving character over the full length of the test section. Momentum thicknesses computed using Eq. (A1) are shown in Fig. A2.

$$\theta = \int_{-\infty}^{\infty} \frac{U(z) - U_1}{U_2 - U_1}\left(1 - \frac{U(z) - U_1}{U_2 - U_1}\right) \mathrm{d}z \tag{A1}$$

An empirical relation for the growth rate of an unconstrained shear layer is given by Eq. (A2) [23]:

$$\frac{\delta_\omega}{x} = 0.085\frac{(1-r)(1+s^{0.5})}{1+rs^{0.5}} \tag{A2}$$

Because both the momentum and vorticity thicknesses grow linearly with downstream distance, they are related by a simple constant that is dictated by the velocity profile of the shear layer. For an error-function approximation to the canonical shear-layer velocity profile

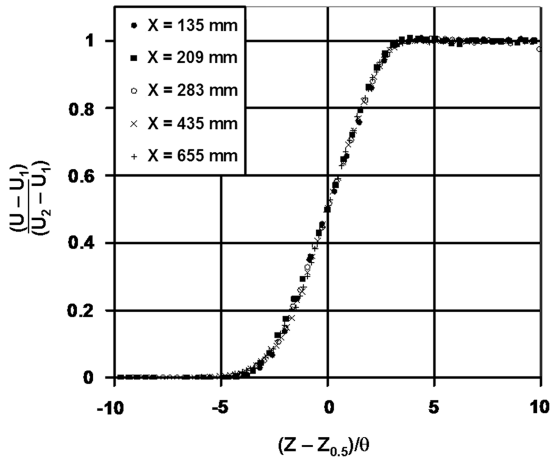

Fig. A1 Nondimensional velocity profiles measured in the CSLWT test section.

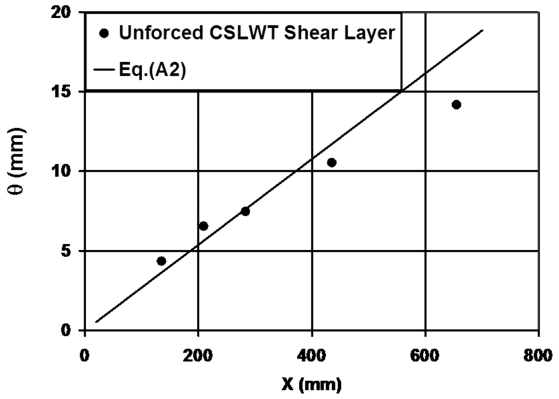

Fig. A2 Streamwise momentum-thickness growth in the CSLWT shear layer.

[8] [Eq. (A3)], the value of this constant can be shown to be approximately 0.2 (i.e., $\theta \approx 0.2\delta_\omega$):

$$\frac{U(z) - U_1}{U_2 - U_1} = 0.5\left(1 + \text{erf}\left(\frac{z - z_{0.5}}{\delta_\omega}\right)\right) \tag{A3}$$

Using $\theta = 0.2\delta_\omega$, the empirical shear-layer growth is included in Fig. A2 and shows good comparison with the momentum-thickness distribution measured in our unforced shear layer up to $x \approx 550$ mm. Downstream of $x \approx 550$ mm, the measured momentum thickness is less than the empirical prediction; this discrepancy may have been caused by the reflection-plane effect of the high-speed test-section wall that may be influencing the growth of the shear layer beyond this point. Despite this discrepancy, the data of Figs. A1 and A2 show that the CSLWT produces a flowfield that is representative of a canonical unconstrained shear layer.

Acknowledgment

These efforts were sponsored by the U.S. Air Force Office of Scientific Research, U.S. Air Force Material Command, under grant FA9550-06-1-0160. The U.S. Government is authorized to reproduce and distribute reprints for governmental purposes notwithstanding any copyright notation thereon.

References

[1] Tyson, R. K., *Principles of Adaptive Optics*, Academic Press, San Diego, CA, 1991.

[2] Cicchiello, J. M., and Jumper, E. J., "Far-Field Optical Degradation Due to Near-Field Transmission Through a Turbulent Heated Jet," *Applied Optics*, Vol. 36, No. 25, 1997, pp. 6441–6452. doi:10.1364/AO.36.006441

[3] Oster, D., and Wygnanski, I., "The Forced Mixing Layer Between Parallel Streams," *Journal of Fluid Mechanics*, Vol. 123, 1982, pp. 91–130. doi:10.1017/S0022112082002973

[4] Weisbrot, I., and Wygnanski, I., "On Coherent Structures in a Highly Excited Mixing Layer," *Journal of Fluid Mechanics*, Vol. 195, 1988, pp. 137–159. doi:10.1017/S0022112088002356

[5] Rennie, R. M., Siegenthaler, J. P., and Jumper, E. J., "Forcing of a Two-Dimensional, Weakly Compressible Subsonic Free Shear Layer," AIAA Paper 2006-0561, Jan. 2006.

[6] Ho, C.-M., and Huerre, P., "Perturbed Free Shear Layers," *Annual Review of Fluid Mechanics*, Vol. 16, 1984, pp. 365–424. doi:10.1146/annurev.fl.16.010184.002053

[7] Ho, C.-M., and Huang, L.-S., "Subharmonics and vortex merging in mixing layers," *Journal of Fluid Mechanics*, Vol. 119, 1982, pp. 443–473. doi:10.1017/S0022112082001438

[8] White, F. M., *Viscous Fluid Flow*, 2nd ed., McGraw–Hill, New York, 1991.

[9] Hugo, R. J., Jumper, E. J., Havener, G., and Stepanek, C., "Time-Resolved Wave Front Measurements Through a Compressible Free Shear Layer," *AIAA Journal*, Vol. 35, No. 4, 1997, pp. 671–677. doi:10.2514/2.156

[10] Papamoschou, D., and Roshko, A., "The Compressible Turbulent Shear Layer: An Experimental Study," *Journal of Fluid Mechanics*, Vol. 197, 1988, pp. 453–477. doi:10.1017/S0022112088003325

[11] Fitzgerald, E. J., and Jumper, E. J., "The Optical Distortion Mechanism in a Nearly Incompressible Free Shear Layer," *Journal of Fluid Mechanics*, Vol. 512, 2004, pp. 153–189. doi:10.1017/S0022112004009553

[12] Freund, J. B., and Wei, M., "Some Small Changes That Make a Mixing Layer Very Quiet," AIAA Paper 2005-0997, Jan. 2005.

[13] Jumper, E. J., and Hugo, R. J., "Quantification of Aero-Optical Phase Distortion Using Small-Aperture Beam Technique," *AIAA Journal*, Vol. 33, No. 11, November 1995, pp. 2151–2157. doi:10.2514/3.12960

[14] Liepmann, H. W., "Deflection and Diffusion of a Light Ray Passing Through a Boundary Layer," Douglas Aircraft Co., Rept. SM-14397, Santa Monica, CA, May 1956.

[15] Browand, F. K., and Weidman, P. D., "Large Scales in the Developing Mixing Layer," *Journal of Fluid Mechanics*, Vol. 76, 1976, pp. 127–144. doi:10.1017/S0022112076003169

[16] Vreman, A. W., Sandham, N. D., and Luo, K. H., "Compressible Mixing Layer Growth Rate and Turbulence Characteristics," *Journal of Fluid Mechanics*, Vol. 320, 1996, pp. 235–258. doi:10.1017/S0022112096007525

[17] Jeong, J., and Hussain, F., "On the Identification of a Vortex," *Journal of Fluid Mechanics*, Vol. 285, 1995, pp. 69–94. doi:10.1017/S0022112095000462

[18] Hugo, R. J., "Quantifying the Spatio-Temporal Effects of Optically Active Turbulent Flowfields on a Coherent Optical Wave," Ph.D. Dissertation, Department of Aerospace and Mechanical Engineering, Univ. of Notre Dame, Notre Dame, IN, 1995.

[19] Nightingale, A. M., Gordeyev, S., Jumper, E. J., Goodwine, B., and Siegenthaler, J. P., "Regularizing Shear Layer for Adaptive Optics Control Applications," AIAA Paper 2005-4774, June 2005.

[20] Chouinard, M., Asghar, A., Kirk, J. F., Siegenthaler, J. P., and Jumper, E. J., "An Experimental Verification of the Weakly Compressible Model," AIAA Paper 2002-0352, Jan 2002.

[21] Duffin, D. A., "Feedforward Adaptive-Optic Correction of a Weakly Compressible High Subsonic Shear Layer," Ph.D. Dissertation, Department of Aerospace and Mechanical Engineering, Univ. of Notre Dame, Notre Dame, IN, 2008.

[22] Lumley, J., "Coherent Structures in Turbulence," *Transition and Turbulence*, edited by, R. E. Meyer, Academic Press, New York, 1981, pp. 215–241.

[23] Dimotakis, P. E., "Two-Dimensional Shear-Layer Entrainment," *AIAA Journal*, Vol. 24, No. 11, 1986, pp. 1791–1796. doi:10.2514/3.9525

A. Tumin
Associate Editor